Water chemistry and $CaCO_3$ dissolution in the saline part of an open-flow mixing zone, coastal Yucatan Peninsula, Mexico

R. K. STOESSELL
W. C. WARD
B. H. FORD*
J. D. SCHUFFERT*

Department of Geology and Geophysics, University of New Orleans, New Orleans, Louisiana 70148

ABSTRACT

Along the Caribbean coast of the Yucatan Peninsula, brackish ground water (mixed fresh water and sea water) is channeled through upper Pleistocene limestone via fracture-controlled caverns. In caves, cenotes, and caletas at Xcaret, Yalku, and Tancah, this open-flow coastal mixing zone comprises three major layers: (1) an upper dilute zone of gradually increasing salinity with depth (slow mixing), (2) a thin intermediate zone of rapidly increasing salinity with depth (rapid mixing), and (3) a lower saline zone of gradually increasing salinity with depth. The intermediate layer occurs at different absolute salinities at different localities, and it generally corresponds to the level of a notch (apparently related to dissolution) in the wall rock of the caverns.

Chemical composition of the mixed ground water is consistent with that predicted from theoretical conservative mixing of fresh-water and sea-water end members sampled in the Yucatan coastal region. Inorganic-C alkalinity, Mg:Ca and Sr:Ca, and $\delta^{18}O$ and $\delta^{13}C$ of the mixed water give no indication of dissolution or precipitation of $CaCO_3$ as the ground water flows rapidly seaward. Field and petrographic observations, however, show that aragonite is preferentially dissolving throughout the modern mixing zone, and in particular in the saline portion.

Comparison of saturation indices to calculated mixing curves shows that the coastal mixing zone of the eastern Yucatan Peninsula is undersaturated with respect to $CaCO_3$ over a wide range of salinity, including mixtures of as much as 95% sea water for aragonite and 90% sea water for calcite. Supersaturation with respect to stoichiometric dolomite is maintained over the whole range of salinities, but supersaturation with respect to calcian dolomite ($Ca_{57}Mg_{43}$) can be confined to high-salinity mixtures, depending on the thermodynamic data base used in calculations. These data suggest that (1) dissolution of coastal limestone can take place in the sea-water–dominated portion of the mixing zone and (2) the mixing-zone model for dolomitization can be extended to much higher salinities than is indicated by the widely accepted "Dorag" model.

INTRODUCTION

The Caribbean coastal region of the Yucatan Peninsula is characterized by abundant cenotes (sinkholes), caletas (rocky inlets), submarine caves, and crescent-shaped beaches, all the result of joint-controlled dissolution of upper Pleistocene limestone (Back and others, 1979, 1986). This rock is a mixture of mainly low-Mg calcite and aragonite, of which the aragonite is dissolving within the zone of mixed fresh and marine ground water (Ward and Halley, 1985; Ford, 1985; Ford and others, 1985; Back and others, 1986).

Previous geochemical models of mixing fresh-water and sea-water end members have emphasized dissolution of calcite (and by implication, aragonite) in the fresh-water portion of the mixing zone (for example, see Badiozamani, 1973). Back and others (1986) calculate that aragonite dissolution occurs within the coastal mixing zone of the eastern Yucatan Peninsula in water compositions less than 60% sea water. In this study, we demonstrate that chemical modeling of the present Yucatecan mixing zone predicts aragonite dissolution in waters approaching sea-water composition. Implications of this study bear on the relative stability of carbonate minerals in the mixing zone and thus on dolomitization and development of secondary porosity in coastal limestone.

Water and rock samples were taken from caves and cenotes in upper Pleistocene limestone at 5 locations along 50 km of the eastern coast of the Yucatan Peninsula (Fig. 1). Sampling was done during the summer dry seasons of 1983 and 1984. At Xcaret and Yalku, detailed sampling of water and adjacent wall rock was done in vertical profiles through the mixing zone. It is important to note that water samples discussed in this paper were taken in or near submarine caves and may not represent pore waters within noncavernous limestone.

Conservative mixing calculations, using end members corresponding to our most dilute (2.8% sea water) and most concentrated (100% sea water) samples, predict the aragonite dissolution observed in the saline portion of the mixing zone. Aragonite dissolution has not significantly changed the bulk chemistry of the water sampled. We believe that this is because of the large water:rock ratio in the submarine caves and the rapid passage (on the order of a day) of this water through the caves. Saturation indices, element concentrations, and C and O isotopes of our mixing-zone water samples are in agreement with modeling of conservative mixing between fresh water and sea water where the fresh-water end member corresponds to fresh water entering the mixing zone along the Caribbean coast of the peninsula.

METHODS

Sampling

At each sampling site (Fig. 1), electrical conductivity and temperature profiles of cave waters were run with a field temperature-salinity-conductivity meter to determine the location of salinity changes within the mixing zone. Most water samples were taken in vertical profiles with an originally designed apparatus (J. D. Schuffert, unpub. data). The device

*Present addresses: (Ford) Westinghouse Hanford Co., P.O. Box 1970, Richland, Washington 99352; (Schuffert) Scripps Institute of Oceanography, University of California, San Diego, La Jolla, California 92093.

Geological Society of America Bulletin, v. 101, p. 159–169, 9 figs., 1 table, February 1989.

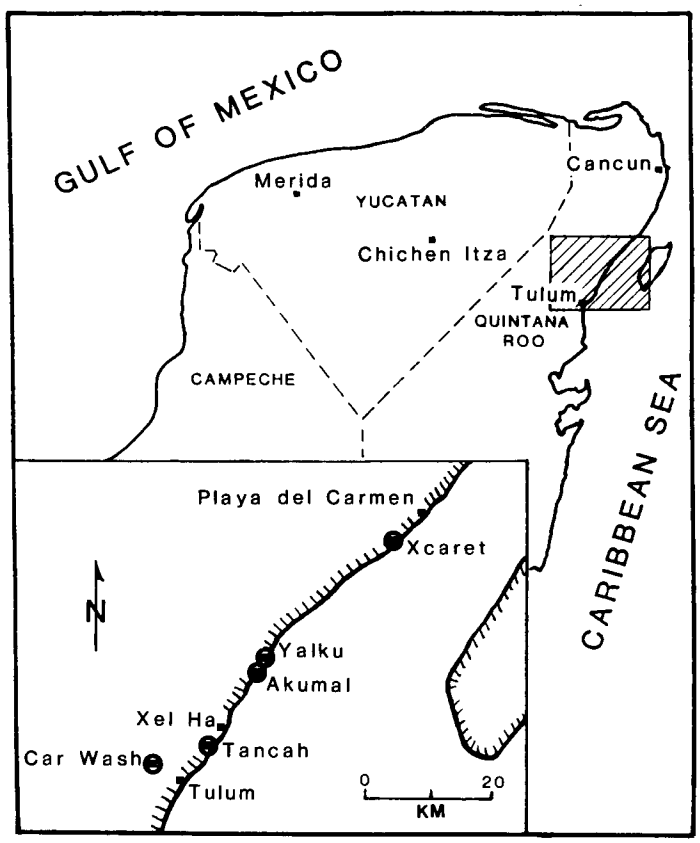

Figure 1. Location map. Hatched rectangle designates portion of northeastern Yucatan Peninsula shown on inset map. Sample locations are marked on inset map by circled squares.

consists of a long aluminum pole with up to eight 0.8-liter polyethylene tubes mounted perpendicular to the pole at 20-cm intervals. The pole was placed by a scuba diver and allowed to sit undisturbd for 20 minutes so that the water column could re-establish itself. Closing of sample tubes was triggered by a diver positioned above and/or downflow of the sampling apparatus.

The samples were processed sequentially, a procedure that took up to two hours for eight samples. All samples were clear solutions lacking turbidity or color. The temperature, pH, and alkalinity were measured, and each sample was filtered through 0.45-μm filter paper. The filtered sample was split into two aliquots, and one of these was acidified with HCl to a pH of about 2. The recorded field pH and temperature represent that of the sample at the time it was removed from the container and may be different from *in situ* values.

An Orion Research 407A pH meter with a combination electrode was used for the pH and alkalinity determinations. The pH meter was calibrated before each sample measurement using pH 4 and 7 buffers. Alkalinity titrations used 0.01 N HCl with a pH end point of 4.5. Over-all accuracy was within ±0.10 pH units (with the exception of the Xcaret samples discussed below) and within ±0.05 meq/l for the alkalinity measurements.

We had difficulty determining an accurate pH with the samples from Xcaret. The same problem occurred, using different electrodes, with Xcaret samples taken in two different field seasons (June 1983 and June 1984). Each pH reading would rise rapidly for about a minute and then appear to stabilize at an initial value. Subsequently, it would slowly drift upward for several minutes before again stabilizing. We interpret the final rise to be due to slow CO_2 degassing. The problem was not apparent in samples from other sites. We used the initial pH values in calculating saturation indices; however, final values also are reported in Table 1.

At Xcaret, Yalku, and Tancah, the wall rock was sampled in vertical profile at 30-cm intervals across the same levels sampled for water. In addition, rock samples were collected above the water table.

Laboratory Analyses

Ca, Mg, Na, K, and Sr concentrations were measured using flame atomic-absorption spectroscopy on filtered, acidified samples. One thousand ppm Sr was added to prevent the formation of Ca and Mg refractory compounds while determining Ca and Mg concentrations in an air/acetylene flame. One thousand ppm alkali elements was added to control ionization in measuring K and Na concentrations in an air/acetylene flame. Sr concentrations were measured in an acetylene/nitrous-oxide flame. Cl and SO_4 were determined on filtered, nonacidified samples. Cl was determined by the Mohr method using a Buchler 4-2500 chloridometer. SO_4 was measured using the $BaSO_4$ turbidimetric method of Tabatabai (1974), and SiO_2 was measured using the standard molybdate-blue colorimetric method. Estimated accuracies are within ±4% for Ca, Mg, Na, K, Sr, Cl, and SiO_2; they were within ±10% for SO_4 concentrations. Compositions of the samples are reported in Table 1.

$\delta^{13}C$ values (relative to PDB) and $\delta^{18}O$ values (relative to SMOW) were measured on the filtered, nonacidified water samples from Xcaret and Yalku by Coastal Science Laboratories, Inc. (Austin, Texas). The estimated precision of the values listed in Table 1 is ±0.2‰. The samples used in the measurements had been stored for up to a year in 250-ml polyethylene bottles. The $\delta^{13}C$ values may have been affected by degassing of CO_2 and subsequent atmospheric exchange during storage. We have not attempted to evaluate the effect of these possible changes, but degassing should increase the $\delta^{13}C$ of the samples. The $\delta^{13}C$ of atmospheric CO_2 is about −7‰ (Hunt, 1979, Fig. 2-3), implying that atmospheric exchange will decrease the $\delta^{13}C$ in the more saline samples of Yucatecan ground water (greater than about 75% sea water) and increase it in the less saline samples (shown below in Fig. 7B).

Rock samples were studied in thin section, using both standard and cathode-luminescence microscopy. Thin sections were stained for Mg calcite, using titan-yellow solution. Bulk-rock mineralogy was determined by comparing X-ray diffraction peak-area ratios to a standard curve constructed using modern Yucatecan carbonate sediments.

Thermodynamic Calculations

Mineral-saturation indices of water samples and those resulting from mixing of end-member fluids were calculated using REACT, a FORTRAN computer program for use on IBM PC- and AT-compatible personal computers (program written by R. K. Stoessell, 1987; the REACT program manual, which gives sources for the thermodynamic data base, is available upon request from the senior author). REACT computes equilibrium assemblages at any diagenetic pressure (P) and temperature (T) in systems involving an aqueous fluid with or without the presence of mineral phases and a gas phase. The program uses the general algorithm described by Reed (1982). Hydrolysis constants of minerals and gases are directly computed in REACT at the PT point of interest using procedures outlined in Helgeson and others (1978, 1981). Activity coefficients of aqueous species, water, and gases are computed, respectively, from the extended Debye-Hückel equation of Helgeson and others (1981), the method of Lietzke and Stoughton (1975), and the modified Redlich-Kwong equation

TABLE 1. YUCATAN DATA

Loc. sample	Depth (m)	%* sea water	T† (°C)	pH† C	Alkal.§ meq/kg H_2O	Cl	SO_4	SiO_2	Ca (mmolal)	Mg (mmolal)	K	Na	Sr	$\delta^{13}C$§§ ppt	$\delta^{18}O$*** ppt	Charge bal. meq/kg H_2O
Car Wash																
CW4	4	2.9	25	6.70	7.14	16.2	0.76	0.070	3.47	2.51	0.26	13.5	0.023	n.m.	n.m.	+0.91
CW7	11	2.8	25	6.90	7.17	16.8	0.74	0.070	3.47	2.47	0.26	13.2	0.014	n.m.	n.m.	0.08
Akumal																
ASB	1	23.8	26.5	6.98	6.10	133.	6.8	0.047	4.73	13.3	2.43	113.	0.014	n.m.	n.m.	1.2
Tancah																
T1	4.4	28.0	27.1	6.85	6.31	156.	7.2	0.054	5.50	16.2	2.74	131.	0.035	n.m.	n.m.	+0.50
T3	4.7	28.1	27.1	6.90	6.04	157.	7.0	0.049	5.44	16.2	2.74	131.	0.033	n.m.	n.m.	+0.04
T5	5.0	28.1	27.1	6.95	5.96	157.	9.3	0.056	5.37	16.3	2.84	134.	0.035	n.m.	n.m.	1.3
T6	5.6	28.3	27.1	6.98	6.09	158.	7.7	0.049	5.42	16.5	2.87	133.	0.033	n.m.	n.m.	+0.29
T7	5.9	28.3	27.1	6.98	5.90	158.	9.0	0.054	5.50	16.3	2.87	131.	0.035	n.m.	n.m.	4.4
T8	6.2	28.7	27.2	6.98	5.76	160.	9.1	0.052	5.40	16.5	2.84	134.	0.036	n.m.	n.m.	3.2
Tancah**																
T7B	5.6	33.3	28	6.84	5.79	186.	8.8	0.052	5.78	19.0	3.08	154.	0.043	n.m.	n.m.	2.7
T8B	6.2	34.2	28	6.90	5.79	191.	8.6	0.051	5.78	19.7	3.05	155.	0.044	n.m.	n.m.	4.9
T9B	6.8	34.2	28	6.90	5.74	191.	8.9	0.052	5.89	20.1	3.14	159.	0.043	n.m.	n.m.	0.33
Xcaret††																
X0	0.1	40.0	27	6.8	5.43	223.	11.2	0.044	6.03	22.1	3.95	192.	0.039	-11.1	3.5	+1.5
X1/2	0.75	40.0	28	6.8	5.38	223.	10.6	0.044	5.98	21.7	3.95	192.	0.039	-10.4	3.4	+1.8
X1	1.7	43.2	28.5	6.9	5.46	241.	12.6	0.041	6.24	24.1	4.44	213.	0.044	-10.3	3.1	+6.5
X2	1.9	59.3	30.5	6.9	4.85	331.	17.0	0.031	7.31	31.2	5.90	276.	0.056	-9.3	2.3	11
X3	2.1	74.7	31.5	6.9	4.05	417.	19.6	0.024	8.40	39.5	7.62	354.	0.070	-7.6	1.5	2.7
X4	2.3	79.6	33	6.9	3.67	444.	22.4	0.014	8.73	43.2	8.08	375.	0.075	-8.1	1.2	5.4
X5	2.5	80.1	33	6.9	3.62	447.	20.5	0.015	8.86	43.6	8.16	381.	0.076	-7.0	1.0	+2.6
X6	2.7	82.8	33	6.9	3.63	462.	20.9	0.014	8.99	44.0	8.29	390.	0.078	-6.8	0.9	3.0
X7	2.9	84.4	33	7.0	3.50	471.	21.7	0.017	9.02	44.5	8.40	399.	0.079	-6.8	0.8	3.3
X8	3.1	86.0	33	7.2	3.42	480.	23.8	0.014	9.08	45.4	8.75	414.	0.080	-6.3	0.9	+0.85
X9	4.25	88.7	28	7.4	3.06	495.	26.3	0.015	9.48	47.1	8.97	421.	0.082	-5.6	0.9	7.4
Yalku																
Y31	0.1	57.4	30	7.0	4.75	320.	15.4	0.037	7.26	30.9	5.85	274.	0.057	-9.5	2.2	+0.73
Y32	0.3	60.4	30	7.1	4.51	337.	15.8	0.037	7.55	32.3	6.06	285.	0.059	-9.8	-2.6	-2.2
Y33	0.5	73.7	30	7.2	3.97	411.	19.1	0.029	8.40	39.2	7.37	337.	0.070	-8.4	-2.0	13
Y34	0.7	82.3	30.5	7.4	3.62	459.	21.1	0.026	8.99	43.2	8.24	391.	0.078	-6.8	1.4	1.0
Y35	0.9	91.4	30.2	7.7	3.13	510.	28.1	0.012	9.61	49.3	9.19	436.	0.086	-5.1	1.1	6.1
Y36	1.1	95.7	30.5	7.7	2.90	534.	29.3	0.014	9.91	50.6	9.60	454.	0.090	-4.6	0.9	11.
Y37	1.3	98.4	30	7.8	2.83	549.	29.7	0.007	10.07	52.4	9.79	459.	0.091	-4.5	0.5	17
Y38	3.0	100.0	30	7.9	2.66	558.	32.3	0.009	10.24	52.8	10.09	473.	0.092	-3.4	0.1	16

Note: This table of data supersedes that reported by Ford (1985, Appendix B, p. 88). Data units reported by Ford should read millimoles/kg of fluid. Samples from Xcaret and Yalku were collected by Schuffert and Stoessel in June 1983; samples from Car Wash, Akumal, and Tancah were collected by Ford and Stoessell in June 1984. Field pH and alkalinity measurements were performed by Stoessell. Isotope measurements were made by Coastal Science Laboratories. All other analytical measurements were made by Schuffert and Ford for the samples which they helped to collect. Estimated analytical accuracies are reported in the text.

*Percent sea water was computed using concentration ratios relative to Y38, our most concentrated sample, which was taken as pure sea water. Sodium ratios were used for the two dilute samples from Car Wash. Chloride ratios were used for the other (more saline) samples.

†As discussed in the text, the temperature is not the *in situ* temperature, but the temperature of the sample at the time the sample pH was measured.

§Carbon alkalinities are the measured alkalinities after subtraction of the "estimated" contributions from boric acid (using the percentage of sea water) and conversion to meq/kg of H_2O.

**Samples T7B, T8B, and T9B were taken on a different day from the other Tancah samples.

††As discussed in the text, the Xcaret samples showed a rise in pH after an initial stabilization. The final pH values for the 11 samples listed in the table are X0, 6.9; X1/2, 6.9; X1, 7.2; X2, 7.4; X3, 7.4; X4, 7.4; X5, 7.4; X6, 7.4; X7, 7.5; X8, 7.6; X9, 7.45.

§§Relative to PDB.

***Relative to SMOW.

of Prausnitz (1969). Thermodynamic dissociation constants of complexes are corrected to the PT point of interest from the vapor-liquid water equilibrium curve using a dielectric constant correction.

The saturation index (SI) of a mineral is the log (Q/K) where Q is the activity product of the hydrolysis reaction and K is the equilibrium constant of the reaction. An example is

$$CaCO_3 + H^+ = Ca^{2+} + HCO_3^-, \text{ for which}$$

$$SI = \log (a_{Ca^{2+}} a_{HCO_3^-} / a_{H^+} K)$$

where "a" represents activity. Due to equilibrium between HCO_3^- and CO_3^{2-}, the SI value is independent of whether the hydrolysis reaction is written to either of these carbonate species.

Errors in SI values for samples are due to (1) analytical errors (discussed above), (2) errors in standard-state thermodynamic data of minerals, (3) errors in dissociation constants of aqueous complexes, and (4) errors in computing activity coefficients (probably insignificant). Merino (1979) has shown that errors in (1) above for major constituents can have an insignificant effect on minor constituents. Our assumption is that the major error is in the previously discussed field pH measurements (up to 0.1 SI units at sites other than Xcaret and possibly greater at Xcaret). Errors associated with (2) are illustrated in Figures 8 and 9 below by the differences (up to 0.25 SI units for calcite and aragonite and 0.5 units for dolomite) in calculated SI values relative to different data bases.

SI values resulting from mixing end-member fluids at 25 °C and 1 atm were computed in REACT, using appropriate amounts (by mass) of each of the aqueous components in the end members. SI values for the field samples were computed in a two-step process, at the measured temperature and at 25 °C. Each sample alkalinity was corrected for estimated boric acid contributions (Stumm and Morgan, 1981), a correction that was significant only for the most *saline* samples. The corrected alkalinity was assumed to be derived from inorganic carbon and was used to estimate total molality of $HCO_3 + CO_3$, required as input in REACT. For pH values approaching that of sea water, the total molality of these species was not precisely equal to the carbonate alkalinity. To determine the precise molality, an equilibrium solution distribution of aqueous species was done at the measured sample T and pH. If the program-computed alkalinity differed from the *corrected* alkalinity, the aqueous equilibrium distribution was rerun using a slightly different total molality of $HCO_3 + CO_3$. After agreement was reached, the equilibrium distribution was rerun at 25 °C and 1 atm, using the correct total molality of $HCO_3 + CO_3$ and total molalities of all other thermodynamic components needed to define the system; for example, total H^+ molality as determined from a hydrogen ion balance at the sample T and pH.

For the SI of a dolomite that might precipitate in the presence of

Yucatecan ground water, we considered the composition of calcian dolomite, $Ca_{1.14}Mg_{0.86}(CO_3)_2$, that occurs in Pleistocene rocks of Yucatan (Ward and Halley, 1985). Such a dolomite is expected to be less stable than a stoichiometric, ordered dolomite, where Ca and Mg atoms are segregated, respectively, into alternate "A" and "B" lattice planes. In sedimentary Ca-rich dolomite, ~20% of the sites in the "A" lattice plane might be occupied by Mg atoms (R. J. Reeder, 1987, personal commun.). This disorder is usually expressed by

$$s = 2\,X_A - 1$$

(Helgeson and others, 1978) where X_A is the mole fraction of the Ca atoms on the "A" lattice plane, and "s" is 1 for total order and 0 for complete disorder. Under this definition, the calcian dolomite of Yucatan could have an "s" value of 0.6.

Stabilities of nonstoichiometric and partially disordered dolomites have been estimated using a Bragg-William approach (Navrotsky and Loucks, 1977) and a tetrahedron approximation of the cluster variation method (Burton and Kikuchi, 1984). The former neglects adjacent-pair interactions, and the latter includes adjacent-pair interactions within and between lattice planes. The latter suffers from the disadvantage of requiring a numerical solution to a series of equations.

In this study, we use the quasichemical pair model "qcpm" of Guggenheim (1952, p. 38–46) to estimate the stability of a dolomite with *excess Ca* and *some disorder*. The method has been previously applied to clay solid solutions (Stoessell, 1981). Our procedure for a calcian dolomite computes adjacent-pair interactions and configurational entropy within each type of lattice plane; those effects are added as a mechanical mixture for the two types of lattice planes. The model is less sophisticated than the approach of Burton and Kikuchi (1984); however, given the unknown effects of lattice defects (for example, see Reeder, 1981) and the disagreement on the stability of ordered stoichiometric dolomite (Carpenter, 1980), it should be adequate for a qualitative discussion.

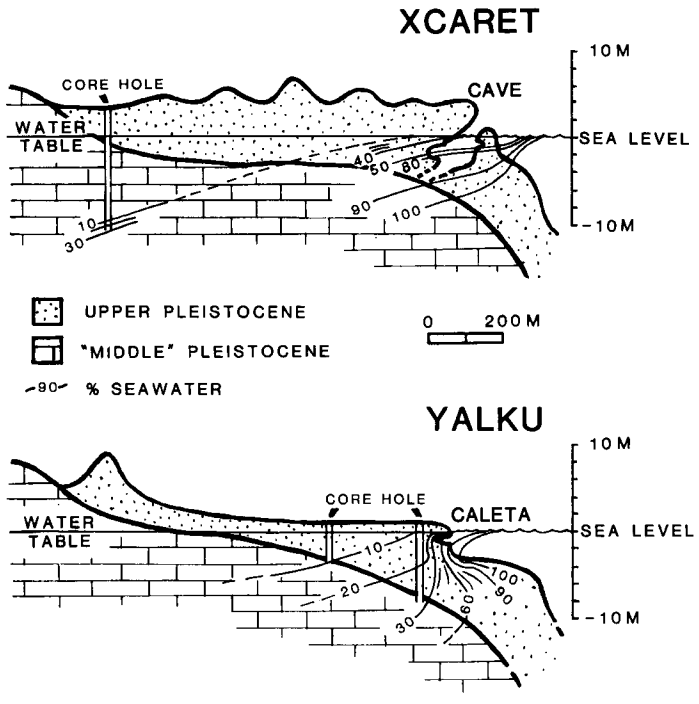

Figure 2. Schematic cross sections at Xcaret and Yalku, showing major rock units and salinity profiles (in percentage of sea water) of coastal ground water.

Our procedure begins with the standard-state free energy of ordered stoichiometric dolomite, corrects this for the presence of excess Ca, and then follows with a correction for disorder. The result gives the following algorithm (modified from Guggenheim, 1952, equation 4.10.9) to predict the $\Delta\bar{G}^\circ_{dol.}$, molar standard-state free energy of formation for a dolomite of composition $(Ca_{X_A}Mg_{(1-X_A)})\,(Ca_{X_B}Mg_{(1-X_B)})\,(CO_3)_2$:

$$\Delta\bar{G}^\circ_{dol.} = \Delta\bar{G}^\circ_{ord.\ stoich.\ dol.} + (X_A + X_B - 1)\,\bar{D}\,(\Delta\bar{G}^\circ_{calcite} - \Delta\bar{G}^\circ_{magnesite}) + RT\left\{\sum_{i=A}^{i=B}(1 - X_i)\ln(1 - X_i) + X_i \ln X_i + 3\left[(1 - X_i)\ln\{[C_i + 1 - 2X_i]/[(1 - X_i)(C_i + 1)]\} + X_i \ln\{[C_i - 1 + 2X_i]/[X_i(C_i + 1)]\}\right]\right\}$$

where $C_i = \{1 + 4X_i(1 - X_i)\,[\exp(2\bar{W}_{Ca,Mg}/6RT) - 1]\}^{1/2}$,

R is the gas constant, T is the temperature in degrees Kelvin, and X_i is the mole fraction of Ca atoms on the ith lattice plane. $\bar{W}_{Ca,Mg}$ is the free-energy difference resulting from taking 3 moles of Ca,Ca interactions and 3 moles of Mg,Mg interactions to form 6 moles of Ca,Mg interactions where the number "6" is the coordination number for adjacent cations. "$\bar{D}$" is a correction factor for error resulting from using the standard-state, free-energy difference of calcite and magnesite to explain the change in free energy due to the presence of excess Ca.

$\bar{W}_{Ca,Mg}$ can be estimated from the relation

$$\bar{W}_{Ca,Mg} = 6RT_c\ln(1.5),$$

from Guggenheim (1952, equation 4.12.13) in which T_c is the critical temperature (°K) marking the equilibrium transition from totally disordered to ordered in stoichiometric dolomite. Using a T_c value of 1150 °C (Reeder and Nakajima, 1982) gives $\bar{W}_{Ca,Mg}$ a value of 6.88 kcal. $\bar{D}$ cannot be evaluated, and so it is set to unity. It should be constant for the amount of excess Ca considered here.

Because there is a difference in opinion of the standard-state free energy of formation of calcite, magnesite, and ordered stoichiometric dolomite, saturation indices for our samples will be referenced to the Yucatecan calcian dolomite composition with respect to data from both Helgeson and others (1978) and Robie and others (1979). These SI values are speculative but do indicate the expected over-all decrease in dolomite stability with increasing compositional variation and disorder.

HYDROLOGY AND PETROLOGY AT SAMPLE SITES

At the four coastal sites (Fig. 1) brackish mixing-zone water passes through enlarged fractures and cave systems at a flow rate of meters per minute. The coastal mixing zone is only a few kilometers wide, implying that water moving through large fractures and caves may cross it in a day. In submarine caves, the brackish ground water flows at high tide over a column of sea water; at low tide, it flows over pockets of sea water stranded in holes. The tidal range was observed to be less than 30 cm at the sample sites. Schematic cross sections of the mixing zone at Xcaret and Yalku are shown in Figure 2.

A turbulent boundary layer, resembling a layer of glycerine, marks the zone where the salinity change with depth is most abrupt (Back and others, 1979, recorded a similar density discontinuity at Xel Ha). Temperature increases rapidly with depth from about 26 to 28 °C across the zone of rapid salinity change from fresh water to sea water (Back and others, 1979, measured similar temperature gradients at Xel Ha). Depth versus salinity profiles at low tide are shown in Figure 3, using data from Table 1. With the exception of the Car Wash samples, these profiles are affected by

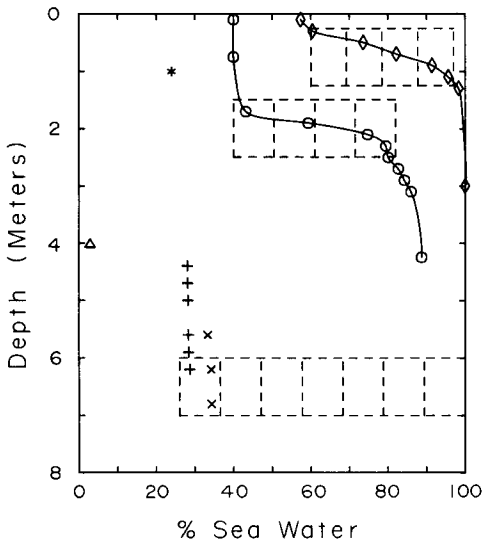

Figure 3. Depth versus percentage of sea-water profiles of samples from the coastal mixing zone: △, Car Wash; *, Akumal; + and x, Tancah; ○, Xcaret; ◊, Yalku. Hatched zones refer to approximate location of notches in wall rock and salinity range of fluids in contact with notches.

the tide, apparently shifting toward higher salinities during high tide (no systematic measurements were made). At the three localities studied in most detail, Xcaret, Yalku, and Tancah (Fig. 1), there is a notch in the cave walls about a meter wide and as much as a meter deep. The general level of the notch corresponds to the greatest change in salinity with depth within the present mixing zone (Fig. 3). This rapid change in salinity occurs over different salinity ranges at the different localities, depending on the distance inland and the local hydrologic flow regime.

Xcaret

Xcaret cave is located at the end of a dirt road that leaves Highway 307 at Xcaret 6.5 km south of Playa del Carmen. This open cave connects through a 3-m-diameter subaqueous passageway to a narrow caleta that lies 50 m seaward of the Xcaret cave. The caleta opens into the Caribbean Sea about 150 m from its landward end.

Water flowing through the caverns is separated into three layers. A thick layer of cool, brackish water 1.5–2 m thick overlies a meter-thick zone of increased temperature and salinity gradient, which, in turn, overlies slightly warmer water of near–sea-water composition. The cave water varied in composition, when we determined it, from 40% sea water at the surface to more than 90% sea water at a depth of 4 m (Fig. 3) at low tide. The water surface in the cave was no more than a few centimeters above sea level, and it fluctuated less than 0.3 m during normal tidal changes.

The caleta and caves at Xcaret are developed in uppermost Pleistocene limestone that retains some original "metastable" mineralogy (aragonite and traces of Mg calcite). Aragonitic components are corals, mollusks, and the green alga *Halimeda*. Calcitic (originally Mg-calcitic) grains are echinoids, coralline red algae, and encrusting and benthic foraminifers. Matrix mud and internal sediment commonly are rich in tunicate spicules. Common nonskeletal grains are fecal pellets. The rocks are mostly skeletal grainstone and packstone with patches of wackestone and coral boundstone, all of which were deposited in the outer lagoon just behind a shelf-margin reef tract. Generally sorting is poor, and grain size ranges from boulder to mud. Judging from outcrop observation and from thin-section petrography, porosity and permeability are erratic in amount and in distribution. Megaporosity estimated from thin sections ranges from about 20% to 60%.

Most diagenetic features of these rocks can be attributed to vadose diagenesis during the late Pleistocene. Cements typically are irregular encrustations of nonluminescent microcrystalline to finely crystalline calcite with scattered needle-fiber calcite. Root traces, microcrystalline-calcite

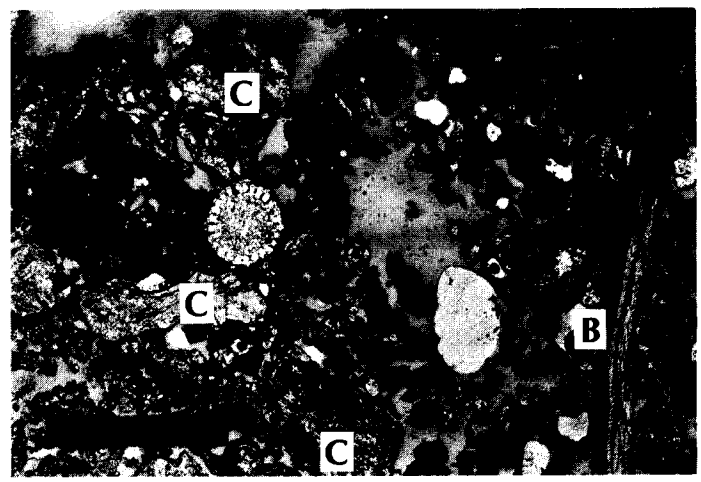

Figure 4A. Plane-light photomicrograph of upper Pleistocene skeletal grainstone from wall rock of Xcaret Cave 30 cm above the water table. Aragonitic grains, such as the coral fragments (C) and bivalves (B), are only slightly dissolved. Light gray background is pore space. Bar scale equals 100 microns.

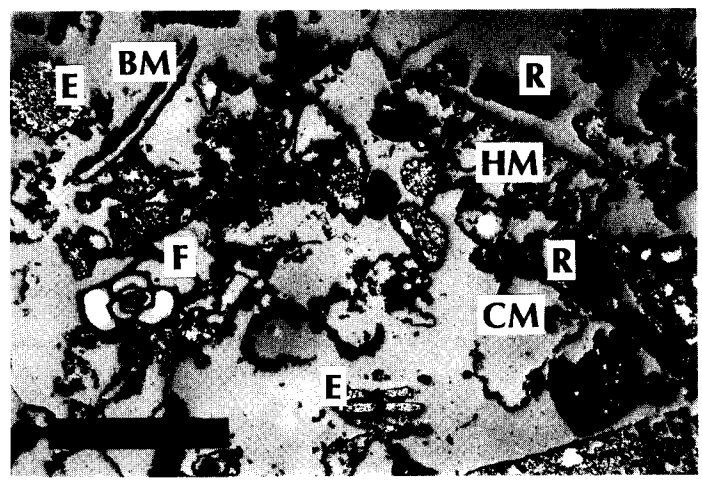

Figure 4B. Plane-light photomicrograph of upper Pleistocene skeletal grainstone from wall rock of Xcaret Cave 1.2 m below the water table. Aragonitic grains are removed by dissolution, leaving numerous micrite-lined molds (for example, *Halimeda* molds, HM; bivalve molds, BM; and probable coral-fragment molds, CM). Calcitic grains (for example, foraminifers, F; red algae, R; and echinoid spines, E) are preserved. Light gray background is pore space. Bar scale equals 100 microns.

root-hair sheaths, and alveolar fabric are common. Small amounts of equant and dog-tooth sparry calcite cement and thin overgrowths on echinoid fragments, precipitated before the vadose cements, record a short period of fresh- or mixed-water diagenesis soon after deposition. These presumably phreatic cements have very thin zones of bright yellow luminescence. The carbonate-mud matrix and some calcitic fossils in these limestones show a dull orange luminescence, suggesting neomorphism of these components.

Intraskeletal aragonite-needle cement (syndepositional cement) is retained in some corals and gastropods. In general, larger fragments of aragonitic corals and mollusks have been slightly to moderately dissolved, and some have been replaced by calcite (neomorphosed). Fine-grained aragonite detritus and some *Halimeda* plates have been totally removed by dissolution. Most components inferred to have been Mg calcite are now calcite, but here and there a few red algae and foraminifers retain some of their original mineralogy. Calcitic skeletal fragments generally are well preserved, but some red algae, foraminifers, and echinoids show effects of partial dissolution, especially in proximity to root traces. The only conclusive evidence of modern precipitation of calcium carbonate is a minor amount of equant Mg-calcite cement (3–6 mole % $MgCO_3$ based on electron-microprobe analysis) and fibrous aragonite cement lining tiny vugs on the surfaces of rock cropping out in the intertidal zone.

In the cave at Xcaret, there is a dramatic difference in diagenesis between the limestone above the water table and that below the water surface (Back and others, 1986, their Figs. 3 and 4). Above the water table, most aragonitic components are only slightly dissolved (Fig. 4A). Preferential dissolution of aragonite, however, is extensive in the subaqueous wall rock (Fig. 4B), which is now adjacent to the mixing-zone cave water (40% sea water near the surface to 89% sea water at 4.2 m; Figs. 2 and 3). Matrix material above the intertidal zone contains as much as 50% aragonite, but carbonate-mud matrix in subtidal wall rock is all calcite. By contrast, most samples of wall-rock matrix from a narrow subaqueous cave only 25 m seaward of the large Xcaret cave are aragonitic (as much as 50% aragonite).

Strongest evidence for on-going dissolution in the larger cave at Xcaret is at 1.5 to 2.5 m below the water surface, where salinity rapidly increases with depth from about 40% sea water to 75% sea water (Fig. 3). At this level, apparently active dissolution is producing a particularly vuggy and "chalky" limestone (Back and others, 1986, their Figs. 6 and 7). The rock is white and clean of modern boring organisms. Within larger vugs, calcitic echinoid spines and carapaces, calcite-replaced mollusk shells, and calcitic fillings of sponge, algal, and fungal borings all stand out in delicate, detailed relief. Fine calcite detritus is accumulating on the floors of the dissolution vugs; aragonite detritus is absent.

Yalku

Caleta Yalku, 2 km northeast of Akumal, also is developed in upper Pleistocene reef rock. The water discharging at the landward edge of this inlet is in the mixing zone, varying from 55% sea water at the surface to 100% sea water at 3 m (Figs. 2 and 3). The layer of mixed water feathers out about 50 m seaward of the inner edge of the caleta. Subaqueous caves 0.5 m below the water table connect the caleta to a series of small cenotes north of the inlet. This cave system is rectilinear, having formed by preferential dissolution along vertical joints and along bedding and/or horizontal fractures just below the water table. The zone of maximum horizontal dissolution lies within the mixing zone (Back, 1985) and is clearly related to the position of the modern water table. Inside the caleta, there are large blocks of limestone, the remnants of collapsed cave roofs.

The composition and diagenesis of the Pleistocene wall rock in the Yalku caleta is similar to that of Xcaret. In contrast to Xcaret, however, there is no strong petrographic evidence for increased dissolution of aragonite in the subaqueous wall rock compared to that in the 0.5-m interval of limestone that lies above the water. Bulk-rock mineralogy within the mixing zone is 15%–50% aragonite and 50%–85% calcite. Limestone above the water is about 35% aragonite and 65% calcite. Below the mixing zone at this site, the wall rock that is exposed to pure sea water retains 10%–20% Mg calcite and as much as 75% aragonite. Bulk-rock mineralogy of upper Pleistocene limestone cored 50 m inland of the Yalku caleta is 30%–75% aragonite and 25%–70% calcite above the water table, but 10%–30% aragonite and 70%–90% calcite below the water table (Rodriguez, 1982).

Tancah

This sample site is a cenote on the western side of the Rancho Tancah coastal road about 2.5 km from its junction with Highway 307 at Km 234. The cenote is part of a large coastal cave system containing numerous sinkholes. It extends to a depth of about 7 m and connects to the Caribbean Sea through an underground passage. At low tide, the salinity of the cenote water was nearly constant over a 7-m depth, about 28% and 34% sea water, respectively, on two different days (Fig. 3). At high tide, however, sea water briefly displaced the brackish water above the floor of the cenote at the mouth of the cave leading to the Caribbean Sea.

Upper Pleistocene limestone at Tancah is composed of peloidal skeletal packstone and wackestone (matrix content is as much as 30 volume %) and skeletal grainstone, which were deposited in an open reef lagoon. Predominant skeletal constituents are *Halimeda*, miliolid and peneroplid foraminifers, red algae, mollusks, echinoids, and small fragments of corals.

Products of pre-Holocene diagenesis of the upper Pleistocene limestone are similar to those in the limestones at Xcaret and Yalku, predominantly nonluminescent vadose cements, including meniscus cement, microcrystalline cement, and calcite needle-fiber cement. These rocks, however, contain more moderately to brightly luminescent columnar and blocky, sparry-calcite cement, presumably the product of phreatic diagenesis during the late Pleistocene. Aragonitic skeletal fragments are

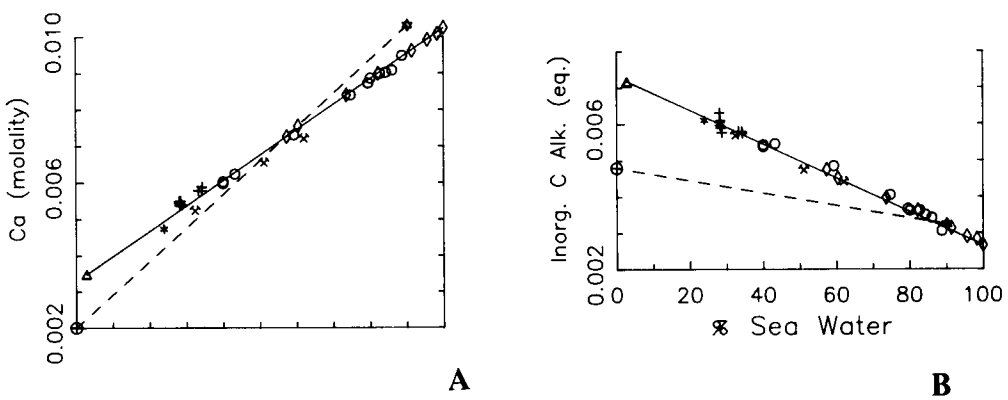

Figures 5A and 5B. Ca molality and inorganic C alkalinity (eq./kg H_2O) of samples versus percentage of sea water (based on Y38 sample as 100% sea water); from this study: △, Car Wash; *, Akumal; +, Tancah; ○, Xcaret; ◊, Yalku and from Back and others (1986): ⊕, Chichen Itza; ✿, Caribbean sea water; ×, Xcaret. Solid line connects end members used in this study; dashed line connects end members used by Back and others (1986).

partly dissolved, and nearly all Mg-calcitic constituents are stabilized to calcite. Aragonitic and calcitic skeletal components were totally dissolved where roots penetrated.

Upper Pleistocene limestones below the modern water table at Tancah (about 30% sea water) show increased postcementation dissolution of aragonite compared to that in the modern vadose zone. Bulk-rock X-ray analysis shows that rock above the water table has 40%–60% aragonite, whereas that below the water has 10%–30% aragonite (original composition of the limestone above and below the water table was similar). In addition, some miliolid and red-algae grains in the vadose-zone rock retain Mg calcite (based on staining with titan yellow), whereas no Mg calcite is retained in samples taken below water. In some samples of submerged rock miliolids, peneroplids, red algae, and echinoids are partly dissolved.

Below a depth of 5 m, wall rock in the Tancah cenote is "middle" Pleistocene skeletal packstone-grainstone. Predominant constituents are benthic foraminifers and red algae. Mollusks are represented by skeletal molds; nearly all aragonitic fragments are removed by dissolution. Bulk-rock X-ray analysis shows 2%–5% aragonite and no Mg calcite. At a depth of 7 m below water level, around the opening of the tunnel connecting to the sea, a notch is formed in vuggy, "chalky" wall rock. Here water composition changes for less than an hour during high tide from about 30% to pure sea water.

"Car Wash"

The "Car Wash" locality is in a fresh-water cenote on the southwestern side of the Coba Highway 5.5 km northwest of its intersection with Highway 307 at Tulum and about 6 km inland from the coast. This cenote connects with subaqueous caves containing abundant speleothems. Water in the cenote had a uniform composition of 3% sea water over an 11-m depth (Table 1).

Wall rock in the cenote is "middle" or older Pleistocene packstone, grainstone, and wackestone deposited in an open back-reef lagoon. Common grain types are mollusks, peneroplid and miliolid foraminifers, red algae, and pellets with lesser amounts of echinoids, *Halimeda*, ostracodes, and corals.

These rocks are low-Mg calcite, having lost all of their aragonite by dissolution and neomorphism. Molds of aragonitic fossils are lined with dog-tooth and equant sparry-calcite cement. Some mollusks and corals are partly replaced by calcite (neomorphosed). Where roots have penetrated, root-hair sheaths and alveolar fabric are common. There is no petrographic evidence for dissolution or precipitation of calcite in the modern phreatic water.

Akumal "Sand Boil"

Brackish water (24% sea water) issues from a 0.5-m-diameter vent into the shallow sea about 7 m offshore at Akumal. The submarine spring flows from upper Pleistocene limestone similar to that at Yalku. A water sample was taken here to add to our data on the dilute portion of the mixing zone.

WATER CHEMISTRY

Inorganic-C alkalinities and Ca concentrations versus percentage of sea water in each sample from this study and from Back and others (1986) are plotted in Figure 5 together with a mixing line predicted for conservative mixing of the CW7 sample (most dilute, 3% sea water) and the Y38 sample (100% sea water). With the exceptions of the two dilute samples from the Car Wash cenote, the percentage of sea-water values were based on Cl-concentration ratios relative to sample Y38 (Table 1), which represents 100% sea water. Zero percent sea water is based on extrapolation from the Car Wash samples. In these computations, Na-concentration ratios based on the Na content of Y38 were used to compute sea-water percentage in the Car Wash samples, and the hypothetical 0% sea-water end member is assumed to have no Na and Cl. Na concentrations were used in the dilute samples from Car Wash because they could be more accurately measured than could Cl concentrations.

Figure 6 shows a plot of molar ratios of Sr:Ca and Mg:Ca versus percentage of sea water and the convex mixing curve predicted from conservative mixing of end members CW7 and Y38 (most dilute and most concentrated, respectively). The extension of the mixing curve to 0% sea water is based on the hypothetical 0% sea water extrapolation from CW7.

$\delta^{13}C$ values and $\delta^{18}O$ values for water samples from Xcaret and Yalku are plotted on Figure 7. The concave trend of the sample points approximates curve A, one of three theoretical mixing curves using sample Y38 as the sea-water end member (Fig. 7C). The fresh-water end members of these curves is assigned a $\delta^{18}O$ value of $-5.61‰$, computed from a least-square linear regression of the 11 Xcaret samples (correlation coefficient of 0.994). Three possible $\delta^{13}C$ values were used for the fresh-water end member: $-12‰$, $-13‰$, and $-14‰$, respectively, for curves A, B, and C. Values of $-13‰$ and $-14‰$ were recorded in fresh water near the Yucatan coast by W. Back (1982, unpub. data). Sample data and calculated mixing curves (Fig. 7C) suggest a $\delta^{13}C$ value of about $-12‰$ for the fresh-water end member used in this study. The values for total inorganic carbon used in the mixing-curve calculations include dissolved nonhydrolyzed CO_2 and H_2CO_3, computed during aqueous equilibrium distributions in REACT for samples CW7 and Y38 and estimated by linear regression to 0% sea water.

Figure 8 presents mixing curves for sea water and fresh water at 25 °C and 1 atm relative to saturation indices (SI) for aragonite, calcite, dolomite, and calcian dolomite. The SI values are plotted relative to those predicted from standard-state mineral data of Helgeson and others (1978), Robie and others (1979), Plummer and Busenberg (1982), and this study (calcian dolomite). Mixing-curve computations using the fresh-water end member CW7 took into account the minor sea-water content of this

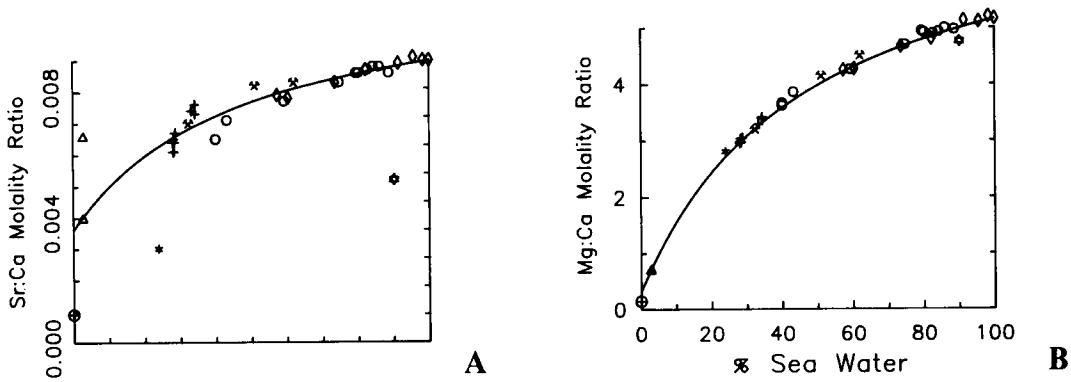

Figures 6A and 6B. Sr:Ca and Mg:Ca molality ratios versus percentage of sea water. The mixing curve was computed using samples CW7 (2.78% sea water) and Y38 (100% sea water). Sample data symbols are those used in Figure 5.

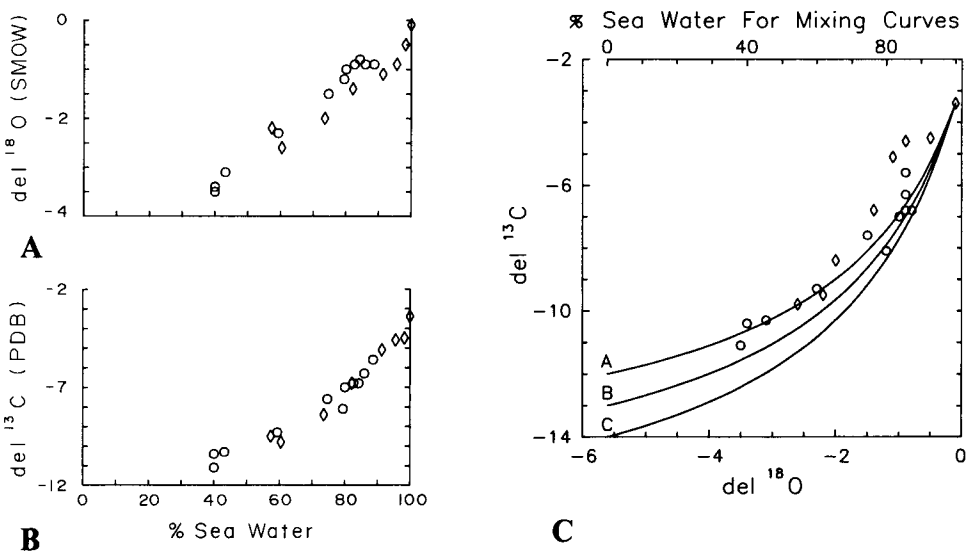

Figures 7A, 7B, and 7C. $\delta^{13}C$ and $\delta^{18}O$ for samples from Xcaret (○) and Yalku (◊). The mixing curves on Figure 7C use sample Y38 as the 100% sea-water end member. The 0% sea-water end members for curves A, B, and C have $\delta^{13}C$ values of $-12‰$, $-13‰$, and $-14‰$, respectively; and a $\delta^{18}O$ of $-5.61‰$, obtained from a linear regression of the Xcaret data.

sample. According to our data (Fig. 8), coastal ground water of the eastern Yucatan Peninsula is undersaturated with respect to aragonite and calcite over a wide range of salinities, including water as much as 95% sea water for aragonite and 90% sea water for calcite (based on SI values of Robie and others, 1979). Even if the SI values of Helgeson and others (1978) are used, this coastal ground water may be undersaturated with respect to aragonite and calcite over 70% of the salinity range (Figs. 8A, 8B). Stoichiometric dolomite supersaturation is maintained over the entire range of salinities (Fig. 8C). The Yucatan coastal ground water is supersaturated with respect to calcian dolomite with the cation composition of $Ca_{57}Mg_{43}$ (like that in upper Pleistocene reefal limestone in the shallow subsurface on the eastern margin of the peninsula; Ward and Halley, 1985) only at mixtures greater than 80% sea water (Fig. 8D, relative to the stoichiometric-dolomite stability of Robie and others, 1979). As discussed above, the salinity range of supersaturation depends on the values used for parameters in the model of the calcian dolomite; however, this range is shifted to high salinities with increased disorder and excess Ca in the dolomite.

DISCUSSION

Diagenesis of Coastal Limestone

Pre-Holocene Diagenesis. At Xcaret, Yalku, Akumal, and the upper part of Tancah, mixing-zone water flows through uppermost Pleistocene limestones. These rocks accumulated 120,000–125,000 yr ago (Szabo and others, 1978) during a highstand of sea level that lasted no more than 6,000 to 10,000 yr (Steinen and others, 1973; Harmon and others, 1983; Harris, 1983). Because of their position near the margin of the shallow shelf, the carbonate deposits at the localities sampled were invaded by ground water flowing from the peninsula for only a short time before the late Pleistocene fall in sea level. When sea level dropped, the platform-margin carbonates quickly passed from the marine- and brackish-phreatic regime into the vadose regime. During late Pleistocene exposure, a dense caliche crust developed over the surface of the subaerial platform, forming an aquitard that directed surface-water flow into sinkholes and open fractures. The caliche "roof" thus helped to protect much of the limestone from extensive vadose diagenesis during the more than 100,000 yr of subaerial exposure. In addition, this runoff flow enhanced dissolution along well-developed joint systems (Weidie, 1986) that would channelize the flow of ground water during the Recent highstand of sea level.

Recent Diagenesis. The upper Pleistocene limestones lay above the water table for about 110,000 yr until the Holocene rise in sea level partly inundated the eastern margin of the Yucatan Peninsula. Today part of this coastal limestone remains above the water table, and part is invaded by brackish (mixed) and saline ground water. The striking difference in diagenesis of upper Pleistocene limestone above the water and that below the water table in the cave at Xcaret (Back and others, 1986) clearly shows that aragonite dissolution is related to the level of the modern mixing zone. No certain evidence for calcite dissolution in this modern mixing zone was found by thin-section or SEM analyses. The horizontal cave systems and large caletas that are related to the present hydrologic setting, however, attest to removal of calcite, presumably by dissolution, in undersaturated fresh and brackish ground water flowing toward the sea (Back and others, 1979, 1986; Hanshaw and Back, 1980).

Water Chemistry

Salinity Profiles. Salinity versus depth profiles in Figure 3 are "nonlinear," reflecting the mechanical stability of an increase in salinity (increasing density) with depth, the absence of turbulence away from the boundary zone (where there is the most rapid change in salinity with depth), and the rapid flow of the overlying fresher water. The salinity profiles (Fig. 3) also show that the salinity range marking the boundary layer is different at different locations.

The position of this boundary layer is marked by a notch in the submarine cave wall. The notch could be due entirely to dissolution; however, the bulk-fluid composition is different in the vicinity of the notch at each of the sample sites. In addition, our data indicate that nearly the entire water column at the various localities was undersaturated with respect to aragonite. J. D. Schuffert (in prep.) suggests that the notch in the submarine cave walls formed by dissolution enhanced by erosion by internal waves propagating along the subsurface density discontinuity in the turbulent boundary layer. One of us (Ward) noted the lack of evidence for physical erosion of the notches. The punky, vuggy wall rock with projections of delicate echinoid spines and fungal-boring molds suggests preferential dissolution of matrix material (that is, chemical, not physical erosion). A similar notch occurs at a rapid salinity change 27 m below the water table in a cenote 22 km inland from the northern coast of the Yucatan Peninsula (E. Perry, 1987, personal commun.). Smart and others (1988) attributed "Swiss cheese" macroporosity at certain levels in wall rock of blue holes in the Bahamas to dissolution in static or slow-moving mixing zones. B. Ward (1987, personal commun.) suggests that rapid

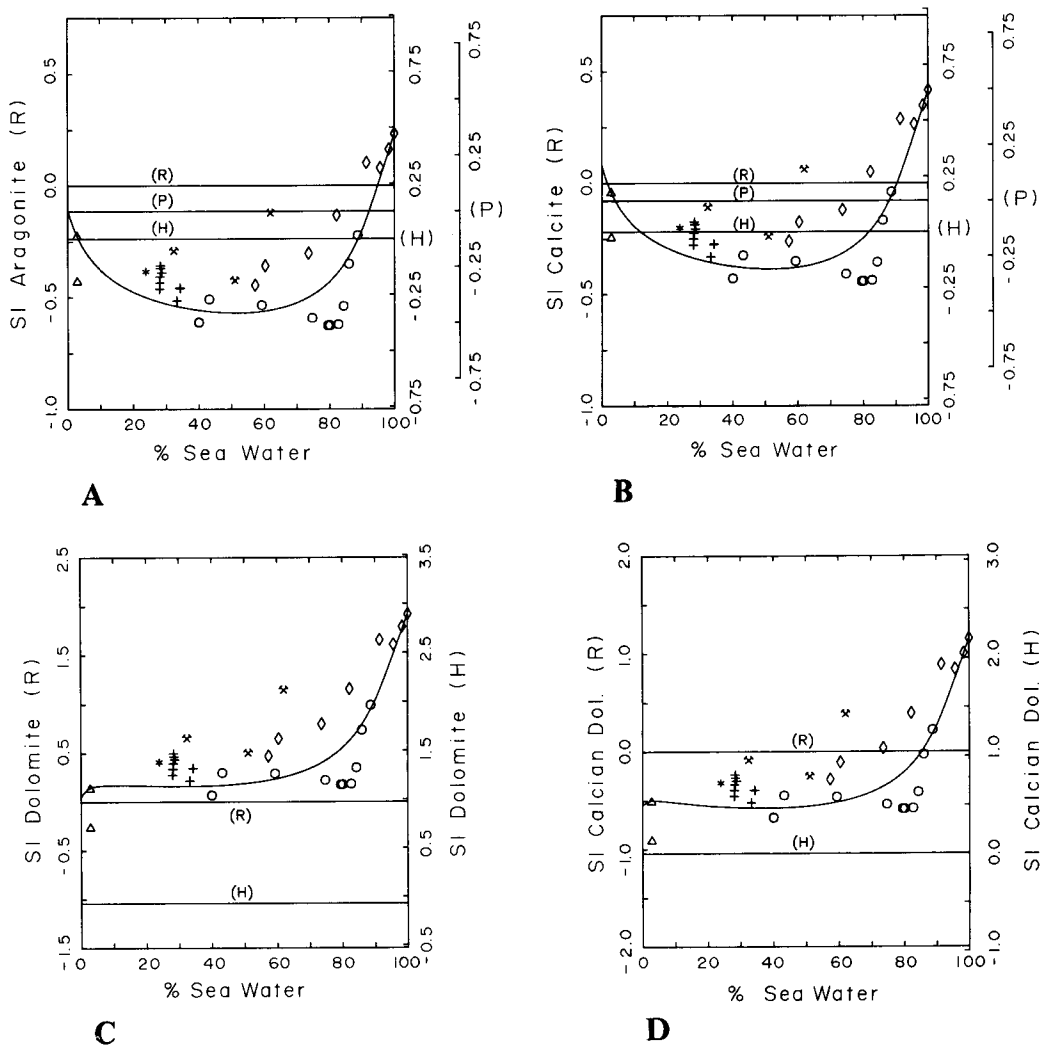

Figures 8A, 8B, 8C, and 8D. 25 °C and 1 atm saturation indices (SI) of samples and mixing curves versus percentage of sea water for aragonite, calcite, stoichiometric dolomite, and calcian dolomite. The solid mixing curve was computed using CW7 (2.78% sea water) and Y38 (100% sea water). Vertical axes and equilibrium lines marked (R), (P), and (H) correspond to SI values relative to standard-state mineral data of Robie and others (1979), Plummer and Busenberg (1982), and Helgeson and others (1978), respectively. Stability data for the calcian dolomite were estimated as described in the text. Sample data symbols are those used in Figure 5.

changes in P_{CO_2} may occur over the intervals of rapid salinity change (that is, zone of most rapid fluid mixing), and perhaps this results in enhancement of carbonate dissolution.

Inorganic-C Alkalinity and Ca Concentration. The linear trend of inorganic-C alkalinity and Ca concentration (Fig. 5) implies that conservative mixing of the most-concentrated sample (Y38) with either of the Car Wash samples (CW4 and CW7) can explain the bulk composition of the water. All of the samples, including the Xcaret samples of Back and others (1986), appear to have common fresh-water and sea-water end members (solid line, Fig. 5). The coastal fresh-water end member (Car Wash 7) has higher alkalinity and Ca than the inland fresh-water end member (Chichen Itza cenote) used by Back and others (1986). These higher values in CW7 probably reflect carbonate dissolution as the fresh water moves from the interior to the edge of the peninsula, where younger limestones contain "metastable" aragonite. In addition, the sea-water end member from Yalku (Y38) is more saline (34.8 ppt) than the Caribbean sea-water end member (31.6 ppt) used by Back and others (1986). Their dilute sea-water end member has higher-than-expected concentration of Ca relative to its salinity.

Mg:Ca and Sr:Ca. Molar ratios of Mg:Ca and Sr:Ca versus percent sea water (Fig. 6) show excellent agreement with that expected from conservative mixing. Both Figures 5 and 6 show that all samples appear to have common end members.

As with inorganic-C alkalinity and Ca concentration (Fig. 5), the Sr:Ca and Mg:Ca ratios in the cave water show no effects of the apparent aragonite dissolution in the wall rock at Xcaret. We believe that this is because of the rapid movement of water in the channels where the samples were taken. Given sufficient time, however, the rock becomes altered by dissolution because of the large volume of water moving through the coastal mixing zone. Presumably the chemistry of *pore* water within the limestone just under the surface of the notch would show the effects of carbonate dissolution.

$\delta^{13}C$ and $\delta^{18}O$. Mixing curves presented in Figure 7C are typical of a water-dominated system (Banner, 1986; Lohmann, 1988). The $\delta^{18}O$ values versus percentage of sea water is a linear relationship (Fig. 7A), as expected in this open-flow system of conservative mixing. The $\delta^{13}C$ values versus percentage of sea water plots as a concave trend (Fig. 7B) because of the greater concentrations of inorganic carbon in the dilute end member relative to the sea-water end member.

Mixing Curves. Six mixing curves for sea water and fresh water at 25 °C and 1 atm are shown in Figure 9 relative to aragonite saturation lines of Helgeson and others (1978), Plummer and Busenberg (1982), and Robie and others (1979). These were computed using three fresh-water end members (the two 3%-sea-water samples from Car Wash, CW4 and CW7; and the Chichen Itza sample from Back and others, 1986) and two sea-water end members (our most saline sample, Y38, and the Caribbean sea-water sample of Back and others, 1986). The percentage of sea-water values on the x axis for each curve is based on the particular sea-water end member used for the mixing curve. Mixing curve A1, relative to the aragonite-equilibrium line of Plummer and Busenberg (1982), corresponds to that used by Back and others (1986), whose calculations use the computer program PHREEQE. The minor differences in our calculations for

curve A1 and the equivalent curve presented in Back and others (1986) presumably reflect the different methods employed to compute activity coefficients in REACT, which uses the extended Debye-Hückel, the equation of Helgeson and others (1981, equation 298), and in PHREEQE, which can use the equation of either Davies (1938) or Truesdell and Jones (1974).

The interesting point of Figure 9 is the large salinity range (70%–90% based on Robie and others, 1979) over which the curves cross above the aragonite-saturation line. The range further increases if we also consider the saturation line based on the data of Plummer and Busenberg (1982) and Helgeson and others (1978). The conclusion drawn by Back and others (1986) that aragonite dissolution at Xcaret should occur only in water less saline than 60% sea water reflects the use of end members that are inconsistent in terms of conservative mixing of the samples taken by them and by us at Xcaret (Figs. 5 and 6). (The effect of using different end members on mixing curves also was demonstrated by Plummer, 1975.) All of the other mixing curves shown on Figure 9 indicate that aragonite may dissolve in more-saline water. Mixing curve B2 (Fig. 8A), calculated using our most dilute sample (CW7) and most concentrated sample (Y38) as end members, predicts aragonite dissolution in water approaching seawater composition.

Fresh-water end member CW7 is in approximate equilibrium with calcite (Fig. 8B), reflecting the reaction with limestone of fresh water moving toward the coast. The source of the fresh water is rainfall, which averages 1 to 1.5 m/yr in the southern part of the peninsula (Back and Hanshaw, 1970). In the dry season, when the samples were taken, fresh water entering the mixing zone is expected to be in approximate equilibrium with calcite. As the volume of fresh water increases during the wet season, more of it may enter the mixing zone undersaturated with respect to calcite. CW4, the other Car Wash sample, is undersaturated with respect to calcite, because its pH is 0.2 units below that of CW7. The bulk compositions of CW4 and CW7 are essentially identical (Table 1), and the lower pH of CW4 may reflect input from soil-derived CO_2 accumulating near the top of the submarine cave at Car Wash.

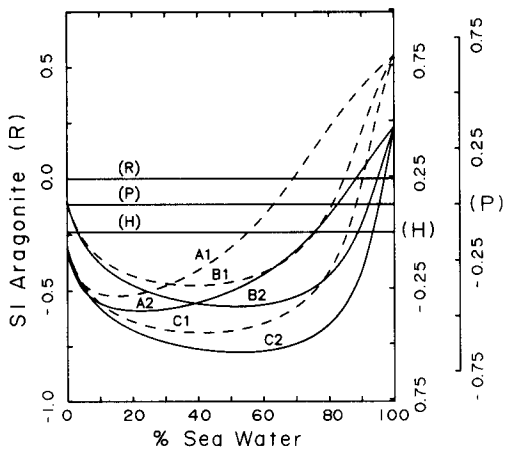

Figure 9. 25 °C and 1 atm saturation indices (SI) for mixing curves versus percentage of sea water using different end members. The letter and number pair marking each mixing curve indicate the dilute end member: A, B, and C, respectively, for Chichen Itza, CW7, and CW4; and the saline end member: 1 and 2, respectively, for Caribbean sea water and Y38. Minor amounts of sea water in samples CW7 and CW4 were accounted for in the mixing curves.

SI of our samples show reasonable agreement with the CW7-Y38 mixing curves (Fig. 8). Differences are thought to reflect errors in the field pH measurements, especially at Xcaret. The three samples from Xcaret reported by Back and others (1986) plot significantly above these mixing curves. The pH values of these samples correspond to the high pH values which we measured at Xcaret after possible degassing of CO_2. Perhaps degassing also explains the high SI values reported by Back and others (1986).

We still have the problem of explaining the preferential preservation of low-Mg calcite in mixing-zone water apparently undersaturated with respect to calcite (Fig. 8B). Our assumption is that this is due to kinetics, related to the smaller degree of undersaturation, and to probable surface poisoning by trace amounts (0.001–0.005 mmolal) of ions, such as phosphate (inorganic phosphorus), which have been shown to reduce calcite dissolution in sea water (Berner and Morse, 1974). Sparse soil in the Yucatan probably allows products of decay such as nitrate and phosphate ions to remain in water entering the subsurface. Back and Hanshaw (1970) reported an average nitrate concentration of 0.25 mmolal in 11 fresh ground-water samples from the interior of the peninsula. Although concentrations of PO_4 were not reported, the fixed ratio of N to P in plant tissue of about 16:1 (Stumm and Morgan, 1981) could result in 0.016 mmolal of phosphate (assuming "congruent" dissolution). This amount should be considered a maximum concentration because PO_4 is usually less mobile than NO_3. In the mixing zone, this concentration would be mixed with 0.002-mmolality phosphate in sea water (Stumm and Morgan, 1981). Further research is needed to determine if these concentrations promote selective dissolution in the mixing zone of Yucatan. Morse and others (1979) reported that aragonite dissolution was unaffected by phosphate in their experiments; however, Walter and Burton (1986) reported that aragonite dissolution is inhibited by the presence of phosphate ions.

Dolomitization. Thus far we have found no evidence for dolomitization in the modern coastal mixing zone along the Caribbean shore of the Yucatan Peninsula. Dolomitic reefal limestone in the shallow subsurface, however, proves that dolomitization (both replacement and cementation) took place along this coast during the late Pleistocene (Ward and Halley, 1985). On the basis of petrographic relationships and O and C isotopes, Ward and Halley (1985) concluded that the calcian dolomite ($Ca_{57}Mg_{43}$) precipitated in the sea-water–dominated portion of the mixing zone.

According to the theory of mixing-zone diagenesis (Hanshaw and others, 1971), dolomite may replace calcite in the presence of fresh-water–sea-water mixtures that are undersaturated with respect to calcite but supersaturated with respect to dolomite. The "Dorag" model (Badiozamani, 1973) predicts dolomitization of limestone (calcite) within the dilute part of the mixing zone (5%–30% sea water). Relative to the data of Robie and others (1979), however, aragonite in the Yucatecan mixing zone is undersaturated in mixtures less than 95% sea water (Fig. 8A), calcite is undersaturated over the range of 5%–90% sea water (Fig. 8B), whereas stoichiometric dolomite is supersaturated over the entire salinity range (Fig. 8C), and calcian dolomite is supersaturated in the high-salinity portion of the mixing zone (Fig. 8D). As pointed out by Hardie (1987), dolomite precipitated in coastal mixing zones is likely to be calcian, not stoichiometric. On the basis of SI derived from the data of Robie and others (1979), calcian dolomite could replace calcite and aragonite only over a narrow range of high-salinity mixtures in the mixing zone of coastal Yucatan. Relative to the data of Helgeson and others (1978), however, aragonite is undersaturated over the range of 3%–88% sea water (Fig. 8A), calcite is undersaturated over 12%–80% sea water (Fig. 8B), and calcian dolomite is supersaturated over the entire salinity range (Fig. 8D).

Considering these saturation indices (Fig. 8) and Mg/Ca ratios (Fig. 6B) and presuming that the modern mixing zone can be used as an

analog for late Pleistocene coastal ground water, the replacement calcian dolomite reported by Ward and Halley (1985) theoretically could have precipitated from the saline portions of the mixing zone. Moreover, the O-isotope compositions of this dolomite ($\delta^{18}O = +1.7‰$) are characteristic of dolomite precipitated in equilibrium with fluids whose isotopic composition is similar to that of the sea-water–dominated portion of the Yucatecan mixing zone, based on fractionation factors presented in Land (1983). A significant point here is that the mixing-zone model for replacement dolomitization can be extended to higher salinities than is indicated by the generally quoted "Dorag" model (Badiozamani, 1973). Furthermore, our data suggest that precipitation of calcian-dolomite cement is favored in the high-salinity part of the mixing zone.

CONCLUSIONS

Composition of mixed ground water in caves, caletas, and cenotes along the Caribbean coast of the Yucatan Peninsula is consistent with that predicted from conservative mixing of fresh-water and sea-water end members sampled in the coastal region. Inorganic-carbon alkalinity, Ca content, Mg:Ca and Sr:Ca ratios, and $\delta^{18}O$ and $\delta^{13}C$ values give no indication of rock-water interaction (dissolution or precipitation) in the mixing zone of this water-dominated system.

Field observations indicate that aragonite is dissolving in the wall rock, especially at Xcaret. Notches (related to dissolution) in the wall of caves and cenotes correspond to the level of the greatest relative salinity change with depth but not to an absolute salinity.

Saturation indices calculated from REACT indicate that Yucatecan coastal ground water can be undersaturated with respect to aragonite and calcite over a wide range of salinity, including water that is as much as 95% sea water for aragonite and 90% sea water for calcite. Supersaturation with respect to stoichiometric dolomite is maintained over the whole range of salinity, but the higher salinity mixtures are most oversaturated with respect to dolomite. Calcian-dolomite supersaturation probably occurs only in the high-salinity portion of the mixing zone. These data suggest that dissolution of aragonite and calcite and precipitation of replacement dolomite and dolomite cement can occur within sea-water–dominated coastal mixing zones.

ACKNOWLEDGMENTS

This paper is based, in part, on the master's theses of Ford and Schuffert. Ford was supported by The Geological Society of America Penrose Grant 3300-84 and grants from ARCO and the Gulf Coast Association of Geological Societies. Schuffert was supported by the U.S. Geological Survey; Shell Oil Company; and the Department of Geology and Geophysics, University of New Orleans. We are grateful to the U.S. Geological Survey for loan of field equipment and for funding some of the analyses.

This study greatly benefited from discussions with Bruce Ward and Bill Back. We are indebted to Phil Choquette, Janet Herman, Bruce Ward, and GSA *Bulletin* reviewers P. Krookneck and D. Whittemore for their very helpful critical reviews of the manuscript.

REFERENCES CITED

Back, W., 1985, Hydrogeology of the Yucatan, *in* Ward, W. C., Weidie, A. E., and Back, W., Geology and hydrogeology of the Yucatan and Quaternary geology of northeastern Yucatan Peninsula: New Orleans, Louisiana, New Orleans Geological Society, p. 99–124.

Back, W., and Hanshaw, B. B., 1970, Comparison of chemical hydrogeology of the carbonate peninsulas of Florida and Yucatan: Journal of Hydrology, v. X, p. 330–368.

Back, W., Hanshaw, B. B., Pyle, T. E., Plummer, N. N., and Weidie, A. E., 1979, Geochemical significance of groundwater discharge and carbonate dissolution to the formation of Caleta Xel Ha, Quintana Roo, Mexico: Water Resources Research, v. 15, p. 1521–1535.

Back, W., Hanshaw, B. B., Herman, J. S., and Van Driel, J. N., 1986, Differential dissolution of a Pleistocene reef in the ground-water mixing zone of coastal Yucatan, Mexico: Geology, v. 14, p. 137–140.

Badiozamani, K., 1973, The dorag dolomitization model—Application to the Middle Ordovician of Wisconsin: Journal of Sedimentary Petrology, v. 43, p. 965–984.

Banner, J., 1986, Petrologic and geochemical constraints on the origin of regionally extensive dolomites of the Mississippian Burlington and Keokuk Formations, Iowa, Illinois, and Missouri [Ph.D. thesis]: Stony Brook, New York, State University of New York, 411 p.

Berner, R. A., and Morse, J. W., 1974, Dissolution kinetics of calcium carbonate in sea water IV: Theory of calcite dissolution: American Journal of Science, v. 274, p. 108–134.

Burton, B., and Kikuchi, R., 1984, Thermodynamic analysis of the system $CaCO_3$-$MgCO_3$ in the tetrahedron approximation of the cluster variation method: American Mineralogist, v. 69, p. 165–175.

Carpenter, A. B., 1980, The chemistry of dolomite formation I: The stability of dolomite, *in* Zenger, D. H., Dunham, J. B., and Ethington, R. L., eds., Concepts and models of dolomitization: Society of Economic Paleontologists and Mineralogists Special Publication 28, p. 111–121.

Davies, C. W., 1938, The extent of dissociation of salts in water. VIII. An equation for the mean ionic activity coefficient of an electrolyte in water, and a revision of the dissociation constant of some sulfates: Journal of Chemical Society, p. 2093–2098.

Ford, B. H., 1985, Geochemistry of water in a coastal mixing zone, northeastern Yucatan Peninsula [M.S. thesis]: New Orleans, Louisiana, University of New Orleans, 90 p.

Ford, B. H., Schuffert, J. D., Stoessell, R. K., and Ward, W. C., 1985, Fluid geochemistry in a coastal mixing zone on the Yucatan Peninsula: Geological Society of America Abstracts with Programs, v. 17, p. 585.

Guggenheim, E. A., 1952, Mixtures: London, England, Oxford Press, 270 p.

Hanshaw, B. B., and Back, W., 1980, Chemical mass-wasting of the northern Yucatan Peninsula by groundwater dissolution: Geology, v. 8, p. 222–224.

Hanshaw, B. B., Back, W., and Deike, R. G., 1971, A geochemical hypothesis for dolomitization by groundwater: Economic Geology, v. 66, p. 710–724.

Hardie, L. A., 1987, Perspectives dolomitization: A critical view of some current views: Journal of Sedimentary Petrology, v. 57, p. 166–183.

Harmon, R. S., Mitterer, R. M., Kriausakul, N., Land, L. S., Schwarcz, H. P., Garrett, P., Larson, G. J., Vacher, H. L., and Rowe, M., 1983, U-series and amino acid racemization geochronology of Bermuda: Implications for eustatic sea level fluctuation over the past 250,000 years: Palaeogeography, Palaeoclimatology, Palaeoecology, v. 44, p. 41–70.

Harris, N. J., 1983, Diagenesis of upper Pleistocene strandplain limestones, northeastern Yucatan Peninsula, Mexico [M.S. thesis]: New Orleans, Louisiana, University of New Orleans, 130 p.

Helgeson, H. C., Delany, J. M., Nesbitt, H. W., and Bird, D. K., 1978, Summary and critique of the thermodynamic properties to rock-forming minerals: American Journal of Science, v. 278-A, p. 1–229.

Helgeson, H. C., Kirkham, D. H., and Flowers, G. C., 1981, Theoretical prediction of the thermodynamic behavior of aqueous electrolytes at high pressures and temperatures. IV. Calculation of activity coefficients, osmotic coefficients, and apparent molal and standard and relative partial molal properties to 600°C and 5 kb: American Journal of Science, v. 281, p. 1249–1516.

Hunt, J. M., 1979, Petroleum geochemistry and geology: San Francisco, California, W. H. Freeman, 617 p.

Land, L. S., 1983, The application of stable isotopes to studies of the origin of dolomite and to problems of diagenesis of clastic sediments: Stable isotopes in sedimentary geology: Society of Economic Paleontologists and Mineralogists Short Course Note Series, No. 10, p. 4.1–4.22.

Lietzke, M. H., and Stoughton, R. W., 1975, The prediction of osmotic and activity coefficients for electrolyte mixtures at elevated temperatures: Oak Ridge, Tennessee, Oak Ridge National Laboratory Report No. 4999.

Lohmann, K. C., 1988, Geochemical patterns of meteoric diagenetic systems and their application to studies of paleokarst, *in* James, N. P., and Choquette, P. W., eds., Paleokarst: Berlin, West Germany, Springer-Verlag, p. 58–80.

Merino, E., 1979, Internal consistency of a water analysis and uncertainty of the calculated distribution of aqueous species at 25°C: Geochimica et Cosmochimica Acta, v. 43, p. 1533–1542.

Morse, J. W., de Kanel, J., and Harris, K., 1979, Dissolution kinetics of calcium carbonate in sea water: VII. The dissolution kinetics of synthetic aragonite and pteropods: American Journal of Science, v. 279, p. 488–502.

Navrotsky, A., and Loucks, D., 1977, Calculation of subsolidus phase relations in carbonates and pyroxenes: Physics and Chemistry of Minerals, v. 1, p. 609–627.

Plummer, L. N., 1975, Mixing of sea water with calcium carbonate ground water, *in* Whitten, E.H.T., ed., Quantitative studies in geological sciences: Boulder, Colorado, Geological Society of America Memoir 142, p. 219–236.

Plummer, L. N., and Busenberg, E., 1982, The solubilities of calcite, aragonite and vaterite in CO_2-H_2O solutions between 0 and 90°C, and an evaluation of the aqueous model for the system $CaCO_3$-CO_2-H_2O: Geochimica et Cosmochimica Acta, v. 46, p. 1011–1040.

Prausnitz, J. M., 1969, Molecular thermodynamics of fluid-phase equilibria: Englewood Cliffs, New Jersey, Prentice-Hall, 523 p.

Reed, M. H., 1982, Calculation of multicomponent chemical equilibria and reaction processes in systems involving minerals, gases and an aqueous phase: Geochimica et Cosmochimica Acta, v. 46, p. 513–518.

Reeder, R. J., 1981, Electron optical investigation of sedimentary dolomites: Contributions to Mineralogy and Petrology, v. 76, p. 148–157.

Reeder, R. J., and Nakajima, Y., 1982, The nature of ordering and ordering defects in dolomite: Physics and Chemistry of Minerals, v. 8, p. 29–35.

Robie, R. A., Hemingway, B. S., and Fisher, J. R., 1979, Thermodynamic properties of minerals and related substances at 298.15 K and 1 bar pressure and at higher temperatures: U.S. Geological Survey Bulletin 1452, 456 p.

Rodriguez, C. J., 1982, Petrology and diagenesis of Pleistocene limestones, northeastern Yucatan Peninsula, Mexico [M.S. thesis]: New Orleans, Louisiana, University of New Orleans, 80 p.

Smart, P. L., Palmer, J. R., Whitaker, F., and Wright, V. P., 1988, Neptunian dikes and fissure fill: An overview of some modern examples, *in* James, N. P., and Choquette, P. W., eds., Paleokarst: Berlin, West Germany, Springer-Verlag, p. 149–165.

Steinen, R. P., Harrison, R. S., and Matthews, R. K., 1973, Eustatic low stand of sea level between 125,000 and 105,000 B.P.: Evidence from the subsurface of Barbados, West Indies: Geological Society of America Bulletin, v. 84, p. 63–70.

Stoessell, R. K., 1981, Refinements in a site-mixing model for illites: Local electrostatic balance and the quasi-chemical approximation: Geochimica et Cosmochimica Acta, v. 45, p. 1733–1741.

Stumm, W., and Morgan, J. J., 1981, Aquatic chemistry: An introduction emphasizing chemical equilibria in natural waters: New York, John Wiley, 780 p.

Szabo, B. J., Ward, W. C., Weidie, A. E., and Brady, M. J., 1978, Age and magnitude of the late Pleistocene sea-level rise on the eastern Yucatan Peninsula: Geology, v. 6, p. 713–715.

Tabatabai, M. A., 1974, Determination of sulfate in water samples: The Sulphur Institute Journal, v. 10, p. 34–36.

Truesdell, A. H., and Jones, B. F., 1974, WATEQ, a computer program for calculating chemical equilibria of natural waters: U.S. Geological Survey Journal of Research, v. 2, p. 233–248.

Walter, L. M., and Burton, E. A., 1986, The effect of orthophosphate on carbonate mineral dissolution rates in seawater: Chemical Geology, v. 56, p. 313–323.

Ward, W. C., and Halley, R. B., 1985, Dolomitization in a mixing zone of near seawater composition, late Pleistocene, northeastern Yucatan Peninsula: Journal of Sedimentary Petrology, v. 55, p. 407–420.

Weidie, A. E., 1986, Fracture density and distribution in folded and horizontal carbonates of northeastern Mexico and Yucatan: Controlling factors in groundwater flow and occurrence: Geological Society of America Abstracts with Programs, v. 18, p. 784.

MANUSCRIPT RECEIVED BY THE SOCIETY DECEMBER 14, 1987
REVISED MANUSCRIPT RECEIVED JUNE 6, 1988
MANUSCRIPT ACCEPTED JUNE 7, 1988

Printed in U.S.A.